# Vertical response of short and long span suspension bridges due to near and far fault earthquakes

Hamed Alizadeh[1], Seyed Hossein Hosseini Lavassani [1*], Ali Masoumi[1]

[1]Faculty of Engineering, Kharazmi University, Tehran, Iran.

Received: 2021/8/11 Accepted: 2021/11/1

## Abstract

Many researches have been currently conducted on the effects of fault distance on structures revealing that their seismic response can differ according to their distance from the fault. Suspension bridges due to their long period and high flexibility can be more sensitive to this phenomenon, especially in vertical vibration. Since the engineers tend to use longer spans, the length factor should be studied more accurately. In this paper, the effects of length factor on the seismic response of the suspension bridge under near and far-fault ground motions were addressed. The Vincent Thomas and Golden Gate suspension bridges as short and long ones, respectively, are selected as the case studies. The seismic responses of two bridges under five main worldwide ground motions contained both near and far-fault ones, with the same peak ground's acceleration, are evaluated. The results indicated that the response of both bridges to the near and far-fault ground motions are perfectly different. Short span suspension bridges are vulnerable to near-fault ground motions, whereas long span ones are completely susceptible to both near and far-fault ground motions, and by increasing the length of span, the sensitivity of bridge was increased against far-fault low frequency excitations. Also, maximum displacement responses of spans in both bridges did not increase by maximizing peak ground's acceleration.

**Keywords:**Near-fault ground motions, Far-fault ground motions, Suspension bridge, Vertical vibration, Length factor.

*Corresponding Author: lavasani@khu.ac.ir

## 1. Introduction

Suspension bridges are highly flexible structures that could be prone to ambient vibrations, such as ground motions, wind and traffic loading. Generally, they vibrate in four lateral, torsional, longitudinal, and vertical modes. Numerical results have indicated that torsional and lateral modes do not occur by themselves. Instead, they are coupled together in the torsional-lateral and lateral-torsional modes, but when a suspension bridge vibrates vertically, it mainly tends to vibrate purely in the vertical mode. However, sometimes the produced response represents several different modes (Huang et al., 2005). A suspension bridge can be excited by support points compressing piers and anchorages. During the excitation process induced by the vertical component of an earthquake, the cable-suspended structure can be vibrated in vertical mode. Also, this vibration might be intensified by the longitudinal excitation of the anchorages and soil-structure interaction (Rubin et al., 1983; Farshi homayoun rooz and Hamidi, 2019). Ground motions can intensely excite the suspension bridges in the vertical mode and their responses could be more remarkable than other structures. Therefore, many methods have been presented to analyze their vertical vibration (Luco and Turmo, 2010).

Nowadays, it is widely accepted that the intense collapses occur in the closer distance to the fault, called near-fault region (Maniatakis et al., 2008). The frequency content of the near and far-fault ground motions is significantly different, so the structures like suspension bridges can exhibit distinctive responses. Therefore, their seismic behavior should be investigated more thoroughly. This investigation could be applied to supplementary topics as well. For example, Rodriguez and Ingham (1995) not only introduced the retrofit of the stiffening truss as the most important part in retrofitting procedure, but also investigated the seismic response of the Golden Gate suspension bridge in the vertical, longitudinal, and transverse modes. Also, they suggested the instruments that reduce the earthquake-induced response by conducting a parametric study on certain types of dampers, and specified their roles in the best performance of the seismic protective system.

Recently, many studies have been conducted to compare the effects of the near and far-fault ground motions on the different structures and their components (Hall et al., 1995; Malhorta,

1999; Ohmachi and Jalili, 1999; Chopra and Chintanapakdee, 2001; Corigliano et al., 2011; Kunnath et al., 2007; Li et al., 2007; Shrestha and Tuladhar, 2012; Zhang and Wang, 2013). Brown and Saiidi (2009) investigated the effects of the near and far-fault ground motions on a substandard bridge bent. The results demonstrated that in comparison to the far-fault ground motions, the near-fault ones caused larger strains, curvatures, and drift ratio in the piers. In another study, Brown and Saiidi (2011) found that the near-fault ground motions lead to more evident failure which could be due to the impulsive effect of the near-fault ground motions. Jia and Ou (2008) evaluated the response of the cable-stayed bridge due to ground motions. The findings showed that for analyzing the bridge, if only the common ground motions are taken into account and pulse-type ground motions are ignored, the response results in substantial underestimation of the potential damage in both horizontal and vertical excitation, especially in the vertical displacement.

Perhaps velocity pulse and fling step are the well-known features amongst all of the characteristics of the near-fault ground motions. Jalali et al. (2012) investigated the three span simply supported bridge under pulse type and permanent-displacement step ground motions. Li et al. (2016) expressed that displacement response of the cable-stayed bridge is large against pulse-type ground motions in compare to none-pulse ones with identical peak ground acceleration (PGA). Also, among two records that each of them contains forward directivity and fling step (with the same PGA) individually, more destructive damages appertain to forward directivity trait. Karaca and Soyluk (2018) introduced the pulse-type ground motion's record more important and destructive than far-fault ones. Also, their conclusion clarified that ratio of the peak ground's acceleration to peak ground's velocity is the critical parameter influencing the effects of the near-fault ground motions on the response of the cable stayed bridge. Cavdar (2012) proved that in spite of having the same PGA, near-fault ground motions make larger displacement and internal force into far-fault ones by a probabilistic sensitivity analysis on the suspension bridge.

Shrestha (2015) investigated the seismic response of the cable-stayed bridges under near-fault ground motions. Results revealed that by maximizing PGA, the maximum response of bridge did not necessarily increase. Also, the vertical ground motions could have profound

effects on the horizontal response. In another study, Soyluka and Karaca (2017) addressed the effects of the near and far-fault ground motions on the suspension as well as cable-stayed bridges, which had nearly the same length. They observed that the displacement response of bridges, especially the suspension ones, to the near-fault ground motions was larger than their response to the far-fault ones.

Erdik and Apaydın (2005) computed the responses of the Bogazici and Fatih Sultan Mehmet suspension bridges to the earthquake loading. They concluded that the vertical vibration of these structures could be caused by lateral excitation, and also, in the torsional-vertical vibration, both torsional and vertical modes could become the dominant modes in response to the vibration. Furthermore, they observed that when the suspension bridges were placed near the fault, more caution should be exercised. Adanur et al. (2012) compared the effect of the near and far-fault ground motions on the geometrically nonlinear behavior of the suspension bridges. They concluded that the maximum moment response of the bridge is produced in the middle point of the deck, and the displacement response varies along the deck. However, both responses were higher under the near-fault ground motions. McCallen et al. (2009) investigated the response of San Francisco Oakland bay suspension bridge to the low frequency near-fault ground motions. They found out that the bridge is quite sensitive to the low frequency components of the ground motions. It should also be noted that by applying a high frequency filter to the ground motions, we can underestimate the response of the structures, especially the ones with long period.

In this paper, the characteristics of the horizontal and the vertical component of the near-fault ground motions are discussed. Then, the behaviors of the short-span and long-span suspension bridges in response to the near and far-fault ground motions are investigated, and subsequently are compared to each other. Ten records are selected from the five worldwide major earthquakes. Each earthquake compresses two records including near and far-fault ground motions. Both records have almost the same PGA. The Vincent Thomas and Golden Gate suspension bridges as the short and long span suspension bridges, respectively, are selected for case studies. After numerical analysis the most outcomes are listed in final part.

## 2. Near-fault ground motions

### 2.1. Horizontal coefficient

The procedure for designing the structures located in the vicinity of the fifteen-kilometers radius of the fault should be considered about near-fault ground motion's effect. There are some specifications, such as directivity, velocity pulse, fling step, hanging wall, and rotational and vertical seismic components that can distinguish the near-fault ground motions from the far-fault ones (Girmaz and Malisan, 2014). In the near-fault ground motions, the horizontal component which is usually normal to the rupture, is stronger than the parallel one.

If the site is in a position, where the fault is moving in its direction, the waves reach each other on the site and cause a big impact, which shortens the arrival time of the waves. This state is called "forward-directivity trait" (Somerville, 2003). If the site is in the opposite direction of the fault movement, the waves get away from each other and their arrival time increases. This condition which is the reverse of the "forward-directivity trait" is called "backward-directivity" (Kalkan et al., 2006), which is less severe. Neuter orientation is a condition in which the receding or acceding fault propagation is not recognizable. In this case, orientation does not affect the amplitude and duration of the time history parameters of the earthquake.

The unique property of the near-fault ground motions is that the arrival of the vertical and horizontal components and their orientations coincide due to the strike slip of the fault. The propagation of the rupture toward the site, with velocity near to the shear velocity, causes to appear the energy of the fault in one large pulse, which has been placed at the beginning of the time history of the velocity records (Makrise and Block, 2004). So, the records which have large pulse at the beginning of the velocity time history can be recognizable as the near-fault ground motions. These records usually specify the horizontal component which is perpendicular to the fault rupture.

Records with "forward-directivity trait" have high frequencies and energy levels that are due to the existence of the pulse. Consequently, the structures having short period are sensitive against these motions. Records which have "backward-directivity trait" have low frequencies

and less energy levels (For further information, see (Alavi and Krawinkler, 2000)). "Fling step" is generally characterized by a unidirectional large-amplitude velocity pulse and the monotonic step in the time history of displacement (Memarpour et al., 2016). This condition can be observed in the strike-slip fault mechanism, and in the strike parallel direction. Moreover, it is not strongly coupled with the forward directivity effect (For further information, see (Kalkan et al. 2006)). This trait is usually attributed to the parallel component of the fault.

## 2.2. Vertical coefficient

The vertical component of the ground motions comprises high frequencies content, clearly seen in the most intense ground motion's records. Theoretically, this can be attributed to the fact that the arrival time of the vertical component and P-waves, propagating vertically in the epicentral region, is the same. P-waves are shorter in length in compare to S-waves. As a result, they contain higher frequencies content (Elnashai and Papazoglou, 2007). PGA is one of the most important properties of the ground motion's records (Colliera and Elnashai, 2010). Usually, the records which are near to the fault contain larger PGA while far ones comprise smaller PGA, this statement is portrayed for Kobe earthquake in Figure1.

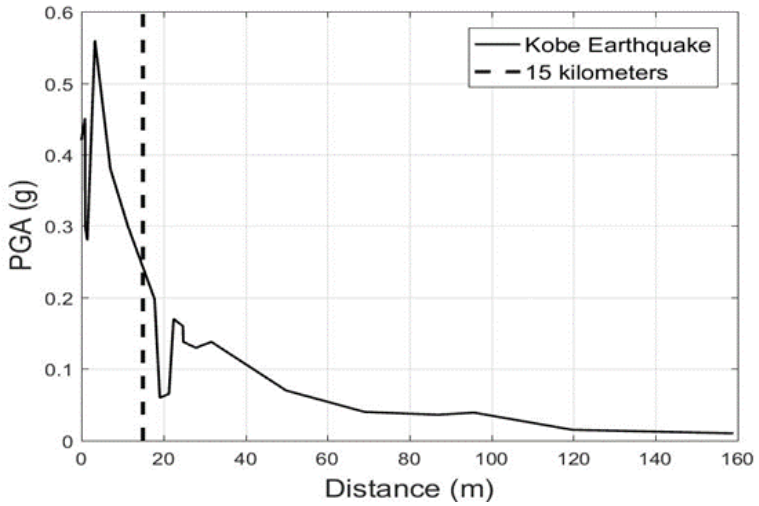


**Fig**. 1 Variation of PGA with respect to its distance from the fault in Kobe earthquake

The vertical component of the ground motions has lower energy content than the horizontal component over the frequency range. However, it tends to concentrate all its energy on a narrow high frequency band, which can be proved by vertically damaging the engineering structures within this range (Elnashai and Papazoglou, 2007).

## 3 .Motion equation of bridge

According to Abdel-Ghaffar and Rubin (1983a), the vibration of a suspension bridge can be divided into two parts: in the first part, the vibration of the pylon-pier system dominates while in the second part the vibration of the suspended structure is dominant, and last part is considered here. Writing the equation of the bridge's motions is an extricated procedure which is not elaborated in detail here. The motion equation can be obtained using kinetic and potential energy, and applying Hamilton's energy principal (For further details, see Abdel-Ghaffar (1979)). Moreover, finite elements method can be used to evaluate the structural parameters like stiffness and mass matrices, in this regard the bridge should be divided into certain finite elements. According to Figure 2, each element contains the main cable, stiffening structure, and at least two hangers and two nodes which are located at the end of element. Each node comprises two degrees of freedom, one of which is the vertical displacement and another one is the bending rotation. The stiffness and mass matrices of each element can be calculated using following equation:

$$[k_{ge}] = \frac{A_1}{30}\begin{bmatrix} 36 & -3L & -36 & -3L \\ -3L & 4L^2 & 3L & -L^2 \\ -36 & 3L & 36 & 3L \\ -3L & -L^2 & 3L & 4L^2 \end{bmatrix}, \quad [k_{cg}]_e = A_2\begin{bmatrix} 12 & -6L & -12 & -6L \\ -6L & 4L^2 & 6L & 2L^2 \\ -12 & 6L & 12 & 6L \\ -6L & 2L^2 & 6L & 4L^2 \end{bmatrix} \tag{1}$$

$$[k_{ce}]_e = A_3 * \left(\sum_{i=1}^{3} A_4 \left[\frac{L}{2}.\frac{-L^2}{12}.\frac{L}{2}.\frac{L^2}{12}\right]\right) * \left(\sum_{i=1}^{3} A_4 \left[\frac{L}{2}.\frac{-L^2}{12}.\frac{L}{2}.\frac{L^2}{12}\right]^T\right) \tag{2}$$

$$[m_t]_e = \frac{A_5}{420}\begin{bmatrix} 156 & -22L & 54 & 13L \\ -22L & 4L^2 & -13L & -3L^2 \\ 54 & -13L & 156 & 22L \\ 13L & -3L^2 & 22L & 4L^2 \end{bmatrix} \tag{3}$$

$k_{cg}, k_{ge}$ and $k_{ce}$ are the gravity stiffness of the cable, elastic stiffness of the girder and cable, respectively. Also, $m_t$ is the mass matrix. In which $A_1, A_2, A_3, A_4$ and $A_5$ are the horizontal cable force per length, bending stiffness of the deck, axial stiffness of the cable, ratio of the dead load to horizontal cable force and multiplication of mass in each element's length $(L)$, respectively. In order to proceed with the analysis, the following assumptions (similar to the assumptions made by Abdel-Ghaffar (1976)) are considered: a) All the existing stresses in the structure obey the Hook's law, so none of the bridge's elements exhibit nonlinear behavior. b) The initial dead load is carried by the main cables and the cross section of the deck does not experience any stress. c) The main cables have constant cross section along themselves and their longitudinal profile is parabolic due to dead load, where the weight of the cables is distributed along the length of the span. d) The hangers are vertical and inextensible, and their forces are considered to be distributed, if the distance is short enough. e) The initial shape of the cross section of the deck remains unchangeable, though due to vibration the cross section may experience the out-of-plane deformation (warping). f) The top of the tower does not resist the displacement. Consequently, the horizontal tension of the cables is the same due to dead load and dynamic load at both sides of the tower. More details of computation are explained by Lavasani et al. (2020a and 2020b) and Alizadeh and Lavasani (2020 and 2021).

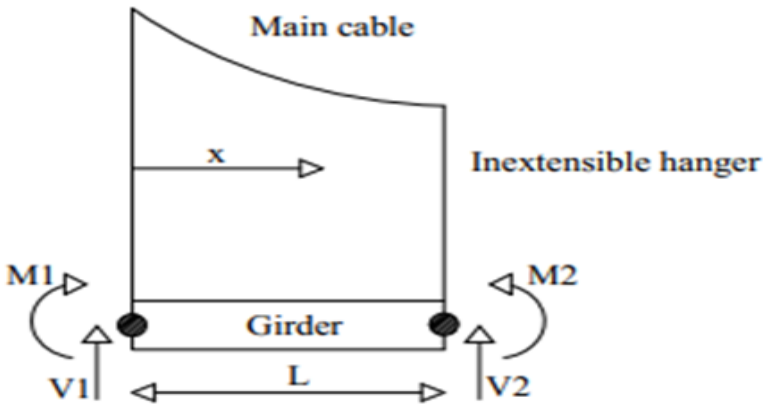


**Fig.** 2 The finite element model of suspension bridge

The motion equation of the bridge can be written as follows (Alizadeh and Lavasani 2020):

$$[\mathrm{M}]\{\ddot{u}(t)\} + [C]\{\dot{u}(t)\} + [K]\{u(t)\} = -[M]\{r\}\ddot{u}_g(t) \quad (4)$$

Where [M], [C], and [K] are the mass, damping, and stiffness matrices of the bridge, respectively. $\{r\}$ is the location vector of the ground acceleration $\{\ddot{u}_g(t)\}$; the vectors $\{\ddot{u}(t)\}$, $\{\dot{u}(t)\}$ and $\{u(t)\}$ are the acceleration, velocity and displacement response of the bridge with respect to the ground motions, respectively. The damping matrix of the bridge is also obtained by means of Rayleigh method using the mass and the stiffness matrices as follows:

$$[C] = a_0[K] + a_1[M] \quad (5)$$

The proportionality coefficients $a_0$ and $a_1$ are computed using the following equation:

$$\frac{1}{2}\begin{bmatrix} \frac{1}{\omega_i} & \omega_i \\ \frac{1}{\omega_j} & \omega_j \end{bmatrix}\begin{Bmatrix} a_0 \\ a_1 \end{Bmatrix} = \begin{Bmatrix} \xi_i \\ \xi_j \end{Bmatrix} \quad (6)$$

Where $\omega_i$ and $\omega_j$ are the natural frequencies of the ith and jth modes of the bridge. In this study, i and j are chosen as the first and tenth vibration modes of the bridge, respectively. Also, $\xi_i$ and $\xi_j$ are equal to 0.4%. To simplify the procedure of the problem solving, the equation is taken into the state-space as follows:

$$\{\dot{Z}\}_{2n\times1} = [A]_{2n\times2n}\{Z\}_{2n\times1} + \{B\}_{2n\times1}(-r)\ddot{u}_g(t) \quad (7)$$

Sub-index $n$ denotes the total degrees of freedom. $Z, A$ and $B$ are the state space vector, state space matrix and input vector, respectively. They can be written as follows:

$$[A]_{2n\times2n} = \begin{bmatrix} 0_{n\times n} & I_{n\times n} \\ -M^{-1}K & -M^{-1}C \end{bmatrix}_{2n\times2n}, \quad \{B\}_{2n\times1} = \begin{Bmatrix} 0_{n\times1} \\ 1_{n\times1} \end{Bmatrix}, \quad Z = \begin{Bmatrix} u(t) \\ \dot{u}(t) \end{Bmatrix}, \quad r = \begin{Bmatrix} 1 \\ \dots \\ 1 \end{Bmatrix}_{n\times1} \quad (8)$$

$I$ is the identity matrix of order n. [0] and $\{0\}$ are the zero matrix and vector with order n×n and n×1, respectively.

$$\{d\} = [C1]\{Z\}, \qquad [C1] = \begin{bmatrix} 1 & \dots & 1 & 0 & \dots & 0 \\ 0 & \dots & 0 & 0 & \dots & 0 \end{bmatrix}_{2*2n} \quad (9)$$

## 4 Numerical analysis

In this section, two suspension bridges having different lengths are considered. In order to accurately investigate the differences between the responses of two bridges, it would be better to have bridges with similar structures. For this purpose, the Vincent Thomas and Golden Gate suspension bridges are selected for case studies. The Vincent Thomas suspension bridge placed between San Pedro and Terminal Island in Los Angeles County, presents a relatively short-span suspension bridge while the Golden Gate bridge located in San Francisco Bay and connector the northern and southern parts, is a long-span one (Abdel-Ghaffar and Rubin (1983b)). According to Figure 3, both bridges meet the already mentioned requirement, i.e. they have two symmetric sides and one central span, steel towers, external anchorages and nearly analogous truss type deck, which is the most important component in the present study. The information of two bridges is provided in Table 1.

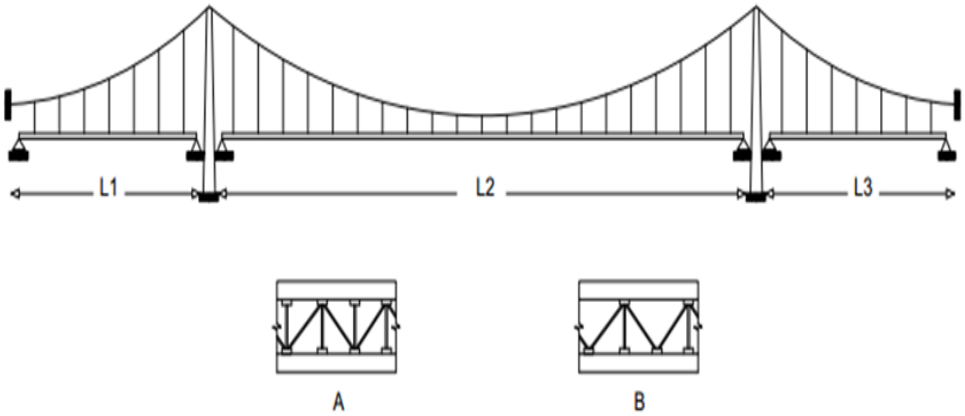


**Fig.** 3 Total structure and deck of (A) the golden gate and (B) the Vincent Thomas suspension bridge

**Table 1** Geometrical and structural parameters of the selected bridges

| Parameter | Golden Gate Bridge | Vincent Thomas Bridge |
|---|---|---|
| Central span length (m) | 1281 | 460 |
| Side span length (m) | 343 | 155 |
| Total dead load of the bridge (kg/m) | 17178 | 5347 |
| Elasticity modulus of the stiffening structure ($N/m^2$) | 200027900100 | 200027900100 |
| Moment inertia of the stiffening structure for side spans ($m^4$) | 1.68 | 0.3749 |
| Moment inertia of the stiffening structure for central span($m^4$) | 2.6 | 0.3729 |
| Horizontal tension of the cable (KN) | 237928 | 30038 |
| Elasticity modulus of the cable ($N/m^2$) | 200027900100 | 186000000000 |
| Cross section area of one cable ($m^2$) | 0.5367 | 0.0781 |
| Virtual length of the cable (m) | 2348 | 1055 |

### 4.1 Free vibration analysis

In order to find the frequencies and mode shapes of the bridges, the eigenvalue problem should be separately solved for each bridge.

$$([K] - \omega^2[M]) \times \{\phi\} = 0 \quad (10)$$

According to the finite element method, the central span of the bridges is divided into 28 elements, while the side spans comprise 11 elements. Figure 4 exhibits the procedure of dividing the whole bridge into finite elements with related degrees of freedom.

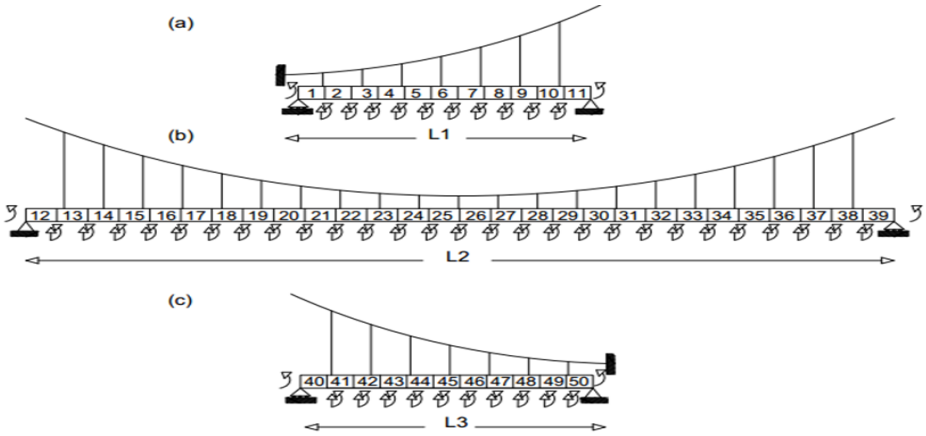


**Fig.** 4 The finite element model of whole bridge, (a) right, (b) center, (c) left span

The computed frequencies and mode shapes of the bridges are provided in Table 2 and Figure 5.

**Table 2** Comparison of frequencies of the selected bridges and their verification

| Mode number | Golden Gate Bridge (rad/s) | Computed by Abdel-Ghaffar (rad/s) | Vincent Thomas Bridge (rad/s) | Computed by Abdel-Ghaffar (rad/s) |
|---|---|---|---|---|
| 1 | 0.59 | 0.6 | 1.23 | 1.24 |
| 2 | 0.77 | 0.77 | 1.38 | 1.38 |
| 3 | 0.97 | 0.92 | 2.16 | 2.18 |
| 4 | 1.13 | 1.14 | 2.17 | 2.18 |
| 5 | 1.28 | 1.28 | 2.9 | 2.88 |
| 6 | 1.6 | 1.6 | 3.42 | 3.46 |
| 7 | 1.8 | 1.8 | 5 | 5.07 |
| 8 | 2.11 | 2.11 | 6.83 | 6.92 |
| 9 | 2.61 | 2.61 | 6.83 | 6.92 |

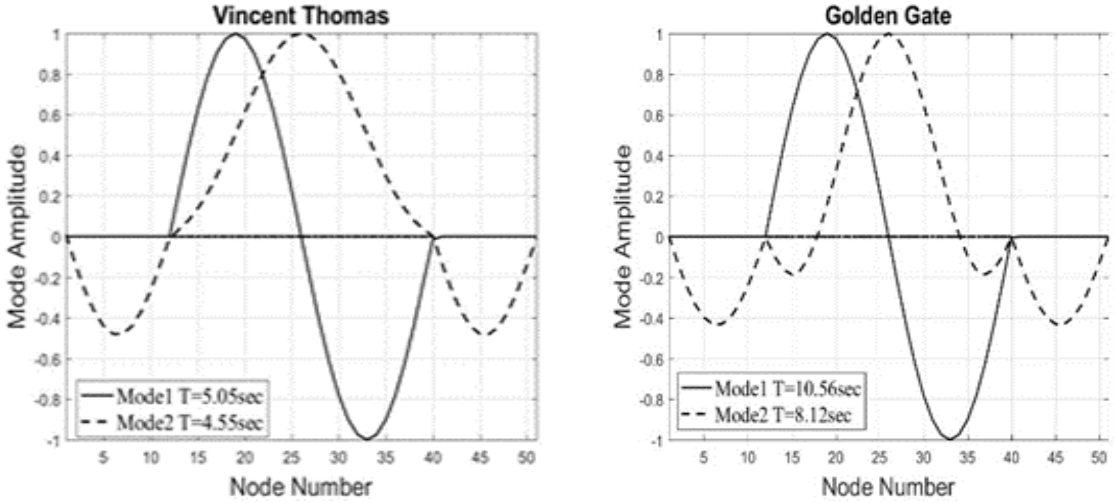


(a) (b)

**Fig**. 5 First three mode shapes of (a) the Vincent Thomas (b) the Golden Gate suspension bridges

In order to address the seismic behavior of the suspension bridges under near and far-fault ground motions, 10 records from the five worldwide major earthquakes are selected, summarized in Table 3. In order to compare the effects of the near and far-fault ground motions, the records are selected in a manner that have nearly the same PGA shown in Figure 6. If the records contain different PGA, then the results do not indicate the trait of the response

and their differences. All the records were downloaded from the PEER ground motion database.

**Table 3** Specifications of the input ground motions

| No. | Earthquake | station name | sort | Distance to fault(km) | Magnitude | PGA | Fault mechanism |
|---|---|---|---|---|---|---|---|
| 1 | Chi-Chi | TCU129 | Near | 1.83 | 7.62 | 0.34 | Revers oblique |
| 2 | Chi-Chi | TCU045 | Far | 26 | 7.62 | 0.34 | Revers oblique |
| 3 | Parkfield | Cholame 6W | Near | 8.16 | 6 | 0.13 | Strike slip |
| 4 | Parkfield | Temblo pre | Far | 15.96 | 6 | 0.13 | Strike slip |
| 5 | Landers | Joshua Tree | Near | 11.03 | 7.28 | 0.18 | Strike slip |
| 6 | Landers | Coolwater | Far | 19.74 | 7.28 | 0.17 | Strike slip |
| 7 | Sanfernando | Lake Hughes | Near | 14 | 6.61 | 0.15 | Revers |
| 8 | Sanfernando | Castic-Old ridge route | Far | 19.33 | 6.61 | 0.17 | Revers |
| 9 | Kocaeli | Izmit | Near | 3.62 | 7.51 | 0.15 | Strike slip |
| 10 | Kocaeli | Fatih | Far | 53.34 | 7.51 | 0.16 | Strike slip |

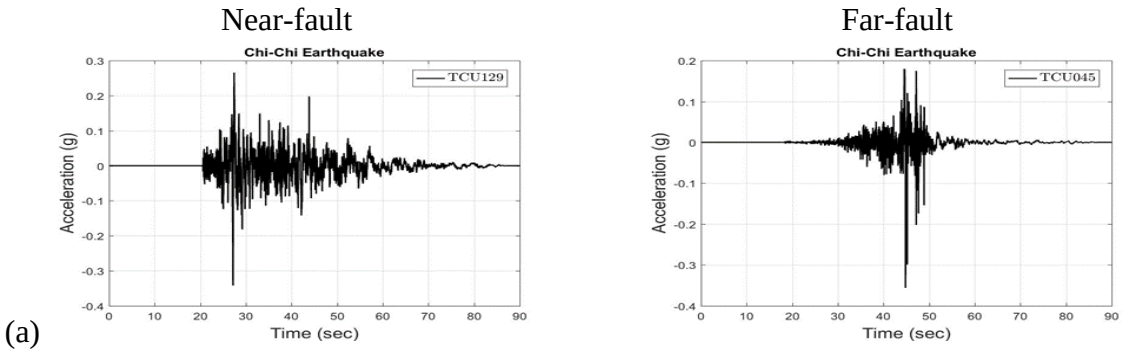

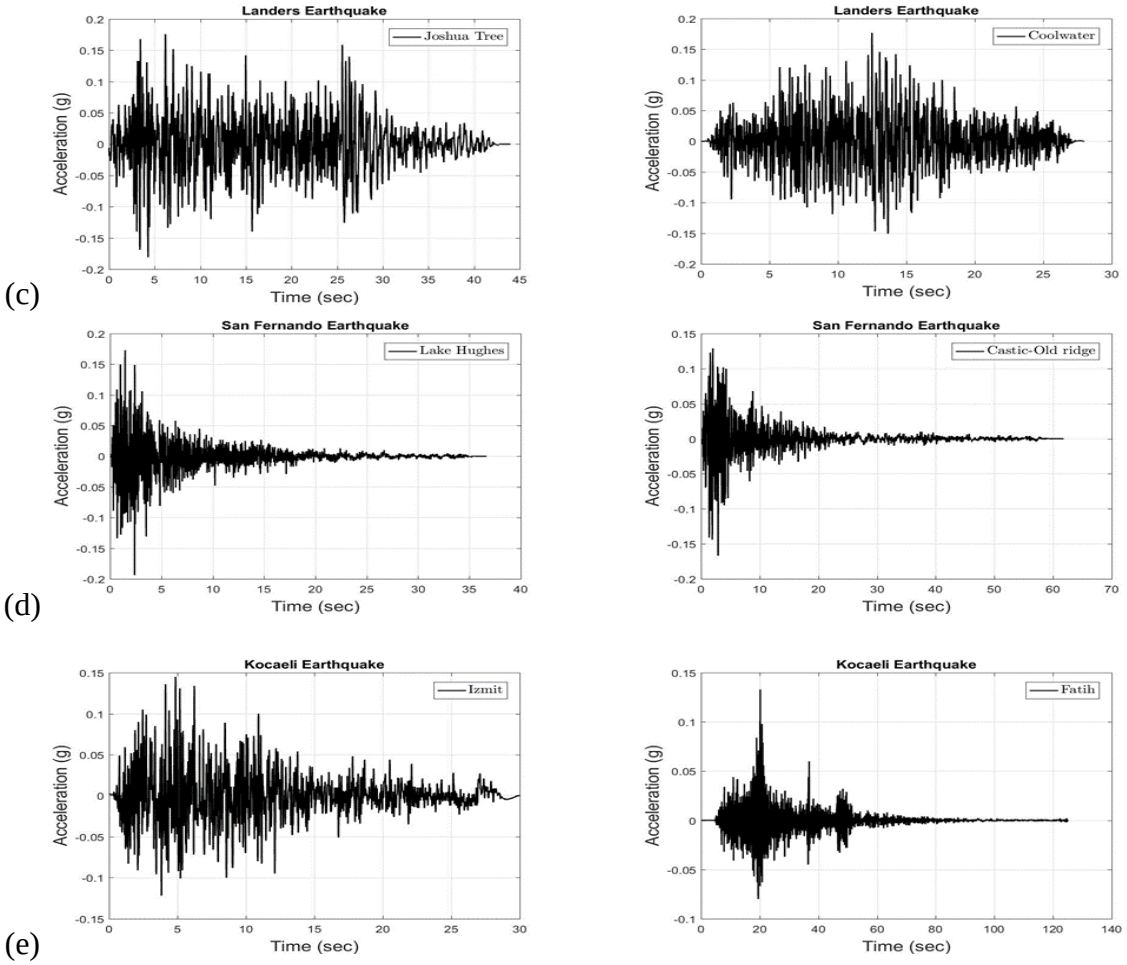


**Fig**. 6 Time history diagrams of the ground motion's acceleration (a) Chi-Chi, (b) Parkfield, (c) Landers, (d) San Fernando, (e) Kocaeli earthquake

Suspension bridges are well-known to have nearly spaced modes. It is rarely observed that a specified mode plays dominant role in producing the ultimate response. It is generally obtained by combining several modes (Murphy and Collins, 2008). Thus, it is necessary to identify the location of the bridge's modes along the frequency content of the ground motion's record to interpret the response. In order to know the frequency content of the selected ground motions, and their effects on the seismic response of the bridges, Fourier transform is needed. Figure 7 demonstrates the Fourier amplitude of the mentioned records and the first frequency of the Vincent Thomas and Golden Gate suspension bridges with FV1 and FG1 as well as the frequency content of each corresponding ground motions, respectively. 50 Hz is the maximum frequency inserted in the horizontal axis. The frequency

of excitation which violates this threshold does not affect the response because the frequency of the last mode of the Golden Gate bridge is nearly 42 Hz, and for the Vincent Thomas bridge, the violated frequency effects are assumed to be negligible.

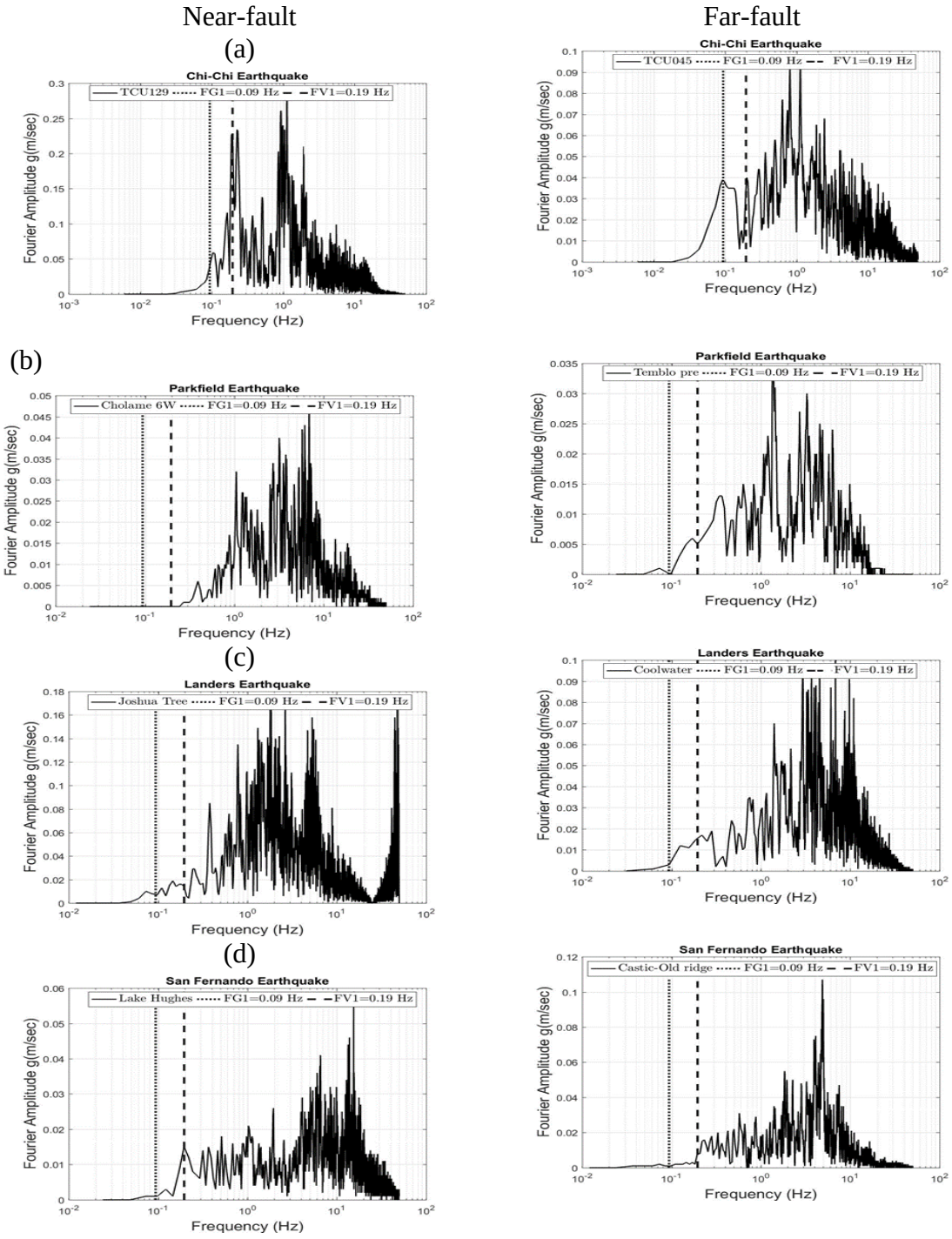

(e)

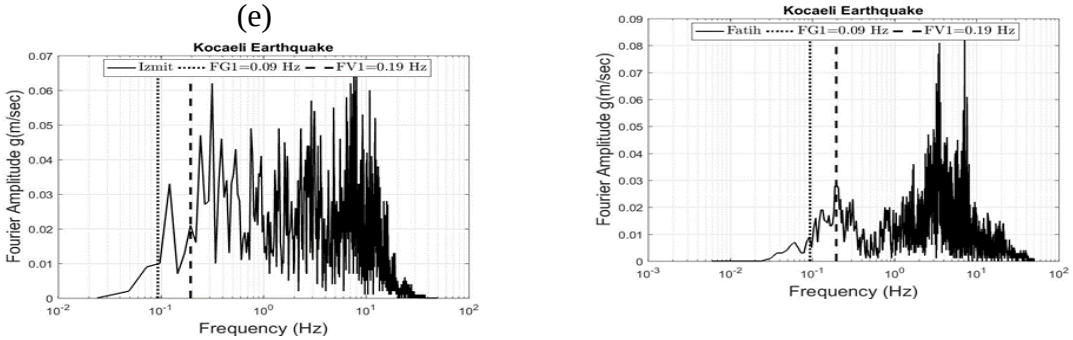


**Fig.** 7 Fourier transform of the selected ground motions (a) Chi-Chi, (b) Parkfield, (c) Landers, (d) San Fernando, (e) Kocaeli earthquake, FG1: The first mode's frequency of the Golden Gate, FV1: The first mode's frequency of the Vincent Thomas suspension bridge

## 5 .Seismic response of the bridge

To investigate the seismic response of the suspension bridges, the selected bridges must have similar systems. That is why only the response of the bridge decks is taken into account. The selected suspension bridges have nearly the same deck shapes. The deck system is truss type and enjoyed enough stiffness in three directions. The load of the ground motions is applied to the vertical degree of freedom of each node. The responses of the Vincent Thomas and Golden Gate suspension bridges under selected records are computed in the state space in MATLAB software R2016b, as previously mentioned. The seismic responses of two bridges to each record (both near and far-fault ground motions) are drown in Figures 8 and 9.

Short-span suspension bridge

(a)

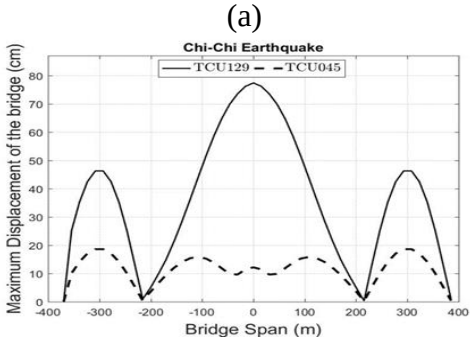


Long-span suspension bridge

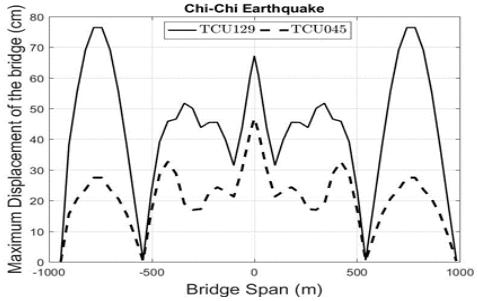

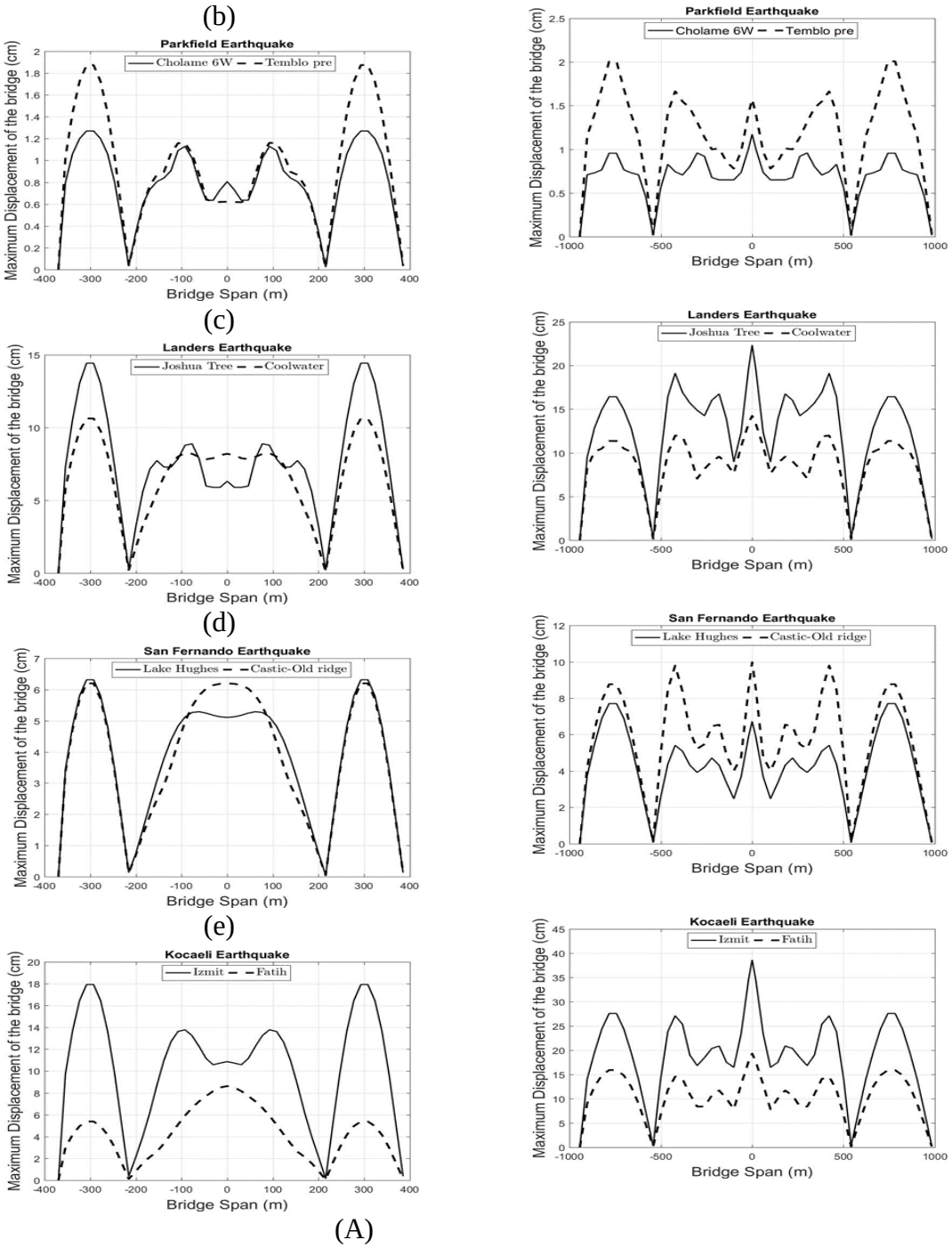


**Fig**. 8 Response of the (A)Vincent Thomas suspension bridge, (B) Golden Gate suspension bridge to (a) Chi-Chi, (b) Parkfield, (c) Landers, (d) San Fernando, (e) Kocaeli earthquake.

### 5.1 Maximum responses

According to Figure 8 section (A), and in part (a), the response of the Vincent Thomas bridge to the near-fault record is extremely larger than far-fault one. This noticeable difference can be justified by the Fourier amplitude of the corresponding records. In Figure 7 part (a), in the near-fault case, the range of variation is between 0-0.3 g(m/s) and there is an abrupt ascending (0.17 g(m/s)) seen around FV1, while in the far-fault case, in spite of reaching the maxima value and ascending in FV1, the ultimate response is much lower due to the presence of a more limited range of variation. In part (b) of Figures 7, which is related to the Parkfield earthquake, in both near and far-fault components, the variation range of the Fourier amplitude is so small that the observed ascending to interrupt FV1 in the far-fault component is negligible although its corresponding response is stronger than the near-fault one. This case demonstrates that 0.1-1 Hz range has apparent effect on the response of the bridge, and each record that has higher Fourier amplitude in this range can cause larger displacement.

Part (c) shows the nearly identical response of the Vincent Thomas suspension bridge to the Landers earthquake's records. Part (c) of Figure 7 exhibits nearly the same maximum point at FV1 in both near-fault and far-fault cases. Similar to the former part, in part (d), both responses are nearly identical in terms of both value and shape. In part (d) of Figure 7, it is clear that there is not any convergence between FV1 and curvature in the near-fault component, but in the far-fault one, the curvature interrupts the FV1 at around 0.01 g(m/s). The variation range of the far-fault case is approximately twice the variation range of the near-fault case. What made the responses to be identical was the low frequency of the ascending curvature, while in the far-fault case, the curvature produced fluctuations with low and almost constant amplitude.

In part (e), a clear difference between near-fault and far-fault responses could be seen again. Part (e) of Figure 7 demonstrates approximately the same range of variation in both near-fault and far-fault components. Although the curvature convergence in the far-fault component exhibits one greater order, its ultimate response places the lowest level of the near-fault component response. This can be due to curvature's ascent in the low frequency

band, and higher number of the bridge modes contribution in the near-fault case, while in the far-fault case, the curvature had descending behavior between FV1 and 1 Hz frequency (which comprises seven modes that are far softer in comparison to higher modes).

According to Figure 8 section (B), and in part (a), there is a significant difference between the near-fault and far-fault corresponding responses. Part (a) of Figure 7 demonstrates the convergence value of about 0.05 and 0.04 g(m/s) in the near-fault and far-fault cases which shows there is not much difference. The difference was mainly caused by the curvature oscillation in low frequency band with larger amplitude in near-fault case (due to the wider range of variation explained in the previous section), which involves the initial modes of the Golden Gate bridge. Part (b) of Figure 8 shows an interesting instance, where the response of the near-fault component is noticeably lower than far one. By noticing part (b) of Figure 7, it is clearly seen that the Fourier amplitude in the near-fault case (in low frequency range) up to about 0.3 Hz is zero, and up to 1 Hz, has much lower values, but in the far-fault case, in addition to the ascending curvature, it fluctuates with large constant amplitude up to 1 Hz, and this is enough to involve major initial modes of the Golden Gate bridge. This case indicates the high sensitivity of the long-span suspension bridge to low frequencies.

Part (c) indicates that in comparison to the far-fault responses, the near-fault responses are placed above the far-fault ones because of the higher curvature convergence and larger amplitude oscillation in low frequency band in the near-fault Fourier amplitude as shown in part (c) of Figure 7. Part (d) demonstrates similar responses to the part (b) with similar reasons. In Part (e) similar to part (a), near-fault response is entirely above the far-fault one. Although according to part (e) of Figure 7, both curvatures are ascending, the corresponding near-fault curvature has large amplitude oscillation in low frequency band.

### 5.3 Middle-point time history response

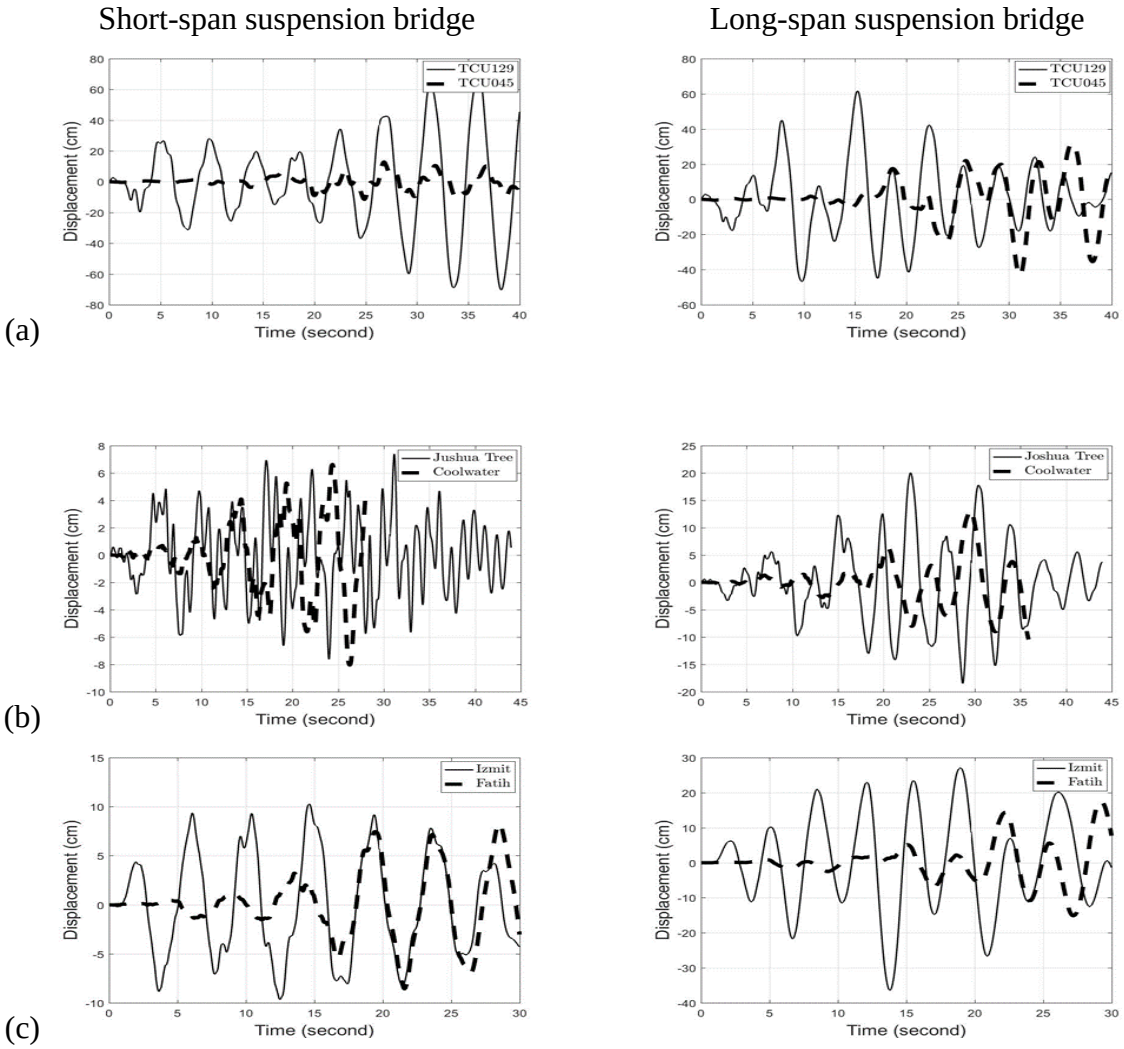


**Fig**. 9 Time history of displacement response to (a) Chi-Chi, (b) Landers, (c) Kocaeli earthquake in their effective time

From part (a) of Figure 9, it is recognizable that both bridges undergo large displacements under near-fault record over time, whereas the far-fault record excites the middle point after its huge spike occurs almost at the end of the effective time as shown in Figure 6(a). According to part (b) of Figure 9, both bridges vibrate for longer period of time due to Landers's near-fault and far-fault records. This event can be attributed to many high

frequency spikes that are shown in Figure 6(c). In part (c) of Figure 9, the near-fault record causes the middle point to vibrate for longer period of time and this is similar to Landers's records, but the far fault, which has a comparatively huge spike, causes displacement after the occurrence of the already mentioned spike, which is more sensible in the Vincent Thomas suspension bridge due to the observed high frequency of this spike. This is clearly apprehensible that the vibration time of the middle point under near-fault ground motions is remarkably longer than far-fault ground motions.

### 5.3 Comparing short-span and long-span bridge responses

According to all parts in Figure 8, it is evident that opposite of the Vincent Thomas bridge, the Golden Gate bridge's response under far-fault components may be strong, but the condition of the near-fault case seems to be more complex. By comparing part (a) of Figure 8, it is found out that the response of the central span of the Vincent Thomas bridge is stronger than the Golden Gate bridge's central span's response, which is almost equivalent to its side spans. Accordingly, in proportion to about 1/3 ratio of central span length, the higher frequencies of the initial modes of the Vincent Thomas can get into resonance along the frequency content of TCU129 record, and as mentioned earlier, a great deal of energy can be transmitted. This statement can be justified by regarding the behavior of the curvature around FG1 and FV1 in part (a) of Figure 7 for TCU129. Therefore, by increasing the PGA, the differences between the central span and the side span's response, in the short-span and long-span bridges, may be increased, respectively.

Mostly, the maximum displacement of the side spans of the short-span bridge is larger than the central span response, but the near-fault and the far-fault components of the Chi-Chi and Kocaeli earthquake demonstrate different states, respectively. As it can be seen in TCU129 and Fatih curvature in Figure 7, when a summit is formed in the vicinity of FV1, the maximum displacement may be happened at the middle point of the central span though with large difference compared to another point. The long-span suspension bridge exhibits a complicated deformation that is due to more spaced modes and their contribution to the ultimate response.

Unlike the short-span bridge that provides a stronger (and at least nearly the same) response to near-fault records, the long-span bridge perhaps represents a stronger response to the far-fault records shown in part (b) and (d) of Figure 8(B). This could be due to the existence of low frequencies in the vicinity of FG1. On the other hand, due to the absence of these frequencies around FG1, the ultimate response can be decreased. Therefore, it can be said that, long-span suspension bridges are perfectly sensitive to low frequencies of ground motions and exerting a high frequency filter results in an imposed underestimation of the response.

## 1. Conclusion

The short and long span suspension bridge's seismic response was addressed in a comparative study. Ten-ground motion's records comprised both near and far-fault records with approximately the same PGA were applied to the Vincent Thomas and Golden Gate suspension bridges as the short and long span bridges, respectively. The responses of the bridges to each ground motion were computed in the state space, and the maximum displacement of the nodes and time history of the middle point of the central span were drawn.

According to the numerical analysis, maximum responses of the nodes variate along the deck in both bridges and are not necessarily larger by maximizing PGA. By increasing the length of the spans, the sensitivity of the bridges to low frequencies rise, so exerting a high frequency filter results in an imposed underestimation of the response and this fact should be attended more meticulously in the far-fault region. Also, far-fault ground motions make larger response in the longer bridges while near-fault ones do not obey certain pattern. In addition, Short span suspension bridges are vulnerable to near-fault ground motions whereas long span ones are completely susceptible to both near and far-fault ground motions. furthermore, near-fault ground motions coerce bridges to vibrate for longer time in compare to far-fault ground motions and also their corresponding response is damped more gradual than far-fault ones which should be attended about fatigue aspect.

## References

1. Abdel-Ghaffar, A. M. (1976). Dynamic analyses of suspension bridge structure. EERL 76-01, California Institute of Technology Pasadena, California.

2. Abdel-Ghaffar, A. M. (1979). Vertical vibration analysis of suspension bridges. Struct Div, 106, 2053-2075.

3. Abdel-Ghaffar, A. M., & Rubin, L.I. (1983a). Vertical seismic behavior of suspension bridge. Earthq Eng Struct Dynam, 11, 1-19.

4. Abdel-Ghaffar, A. M., & Rubin, L.I. (1983b). Nonlinear free vibration of suspension bridges: Applications. Eng Mech, 109(1), 330-331.

5. Adanur, S., Altunis, A., Bayraktar, A., & Akkose, M. (2012). Comparison of near-fault and far-fault ground motion effects on geometrically nonlinear earthquake behavior of suspension bridges. Nat Hazards, 64(1), 595-614.

6. Alavi, B., & Krawinkler, H. (2000). Effects of near-fault ground motions on frame structure. John A. Blume Earthquake Engineering Center,138, Department of Civil and Environmental Engineering, Stanford University.

7. Alizadeh, H., & Lavasani S.H.H. (2020). TMD parameters optimization in different length suspension bridges using OTLBO algorithm under near and far field ground motions. Earthquakes and Structures, 30(5), 625-635.

8. Alizadeh, H., & Lavasani, S.H.H. (2021). Flutter control of long span suspension bridges in time domain using optimized TMD. Int J Steel Struct, 21, 731–742.

9. Brown, A., & Saiidi, M.S. (2009). Investigation of near-fault ground motion effects on substandard bridge columns and bents. CCEER-09-01, Department of Civil Engineering, University of Nevada.

10. Brown, A., & Saiidi, M.S. (2011). Investigation of effect of near-fault motions on substandard bridge structures. Earthq Eng Eng Vib, 10(1), 1-11.

11. Cavdar, O. (2012). Probabilistic sensitivity analysis of two suspension bridges in Istanbul Turkey to near- and far-fault ground motion. Nat. Hazards Earth Syst. Sci., 12(2), 459-473.

12. Colliera, C.J., & Elnashai, A.S. (2010). A procedure for combining vertical and horizontal seismic action effects. Earthq Eng, 5(4), 521-539.

13. Chopra, A.K., & Chintanapakdee, C. (2001). Comparing response of SDF systems to near-fault and far-fault earthquake motions in the context of spectral regions. Earthq Eng Struct Dyn, 30, 1769–1789.

14. Corigliano, M., Scandella, L., Lai, C., & Paolucci, R. (2011). Seismic analysis of deep tunnels in near fault conditions: a case study in southern Italy. Bulletin of earthquake engineering, 9(4), 975-995.

15. Elnashai, A.S., & Papazoglou, A.J. (2007). Procedure and spectra for analysis of RC structures subjected to strong vertical earthquake load. Earthq Eng, 1(1), 121-127.

16. Erdik, M., & Apaydın, N. (2005). Earthquake response of suspension bridge. Vib Prob ICOVP, 181-191.

17. Farshi Homayoun rooz, A., & Hamidi, A. (2019). A numerical model for contribution impact pile driving using ALE adaptive mesh method. Soil dynamic and earthquake engineering, 118: 134-143.

18. Grimaz, S., & MaliSan, P. (2014) Near field domain effects and their consideration in the international and Italian seismic codes. Bollettino di Geofsica Teorica ed Applicata, 55(4), 717-738.

19. Hall, J.F., Heaton, T.H., Halling, M.W., & Wald, D.J. (1995). Near-source ground motion and its effects on flexible buildings. Earthq Spec, 11, 569–605.

20. Huang, M.H., Thabiratnam, D.P., & Perera, N.J. (2005). Vibration characteristic of shallow suspension bridge with pre-tensioned cables. Eng Struct, 27(8), 1220-1233.

21. Jalali, R.S., Jokandan, M.B., & Trifunac, M.D. (2012). Earthquake response of a three-span, simply supported bridge to near-field pulse and permanent-displacement step. Soil Dyn. Earthquake Eng, 43, 380–397.

22. Jia, J.F., & Ou, J.P. (2008). Seismic analyses of long-span cable-stayed bridges subjected to near-fault pulse-type ground motions. In 14th World Conference on Earthquake Engineering, China.

23. Kalkan, E., Eeri, S.M., Kunnath, S.K., & Eeri, M. (2006). Effects of fling step and forward directivity on seismic response of buildings. Earthq Spec, 22(2), 367-390.

24. Karaca, H., & Soyluk, K. (2018). Effects of near-fault and far-fault ground motions on cable stayed bridges. Disaster science and engineering, 4(1), 12-21.

25. Kunnath, S.K., Erduran, E., Chai, Y.H., & Yashinsky, M. (2007). Near-fault vertical ground motions on seismic response of highway overcrossings. Bridge Eng ASCE, 13(3), 282-290.

26. Lavasani S.H.H., Alizadeh, H., & Homami, P. (2020a) Optimizing tuned mass damper parameters to mitigate the torsional vibration of a suspension bridge under pulsetype ground motion: A sensitivity analysis. Journal of Vibration and Control. 26(11-12):1054-1067.

27. Lavasani S.H.H., Alizadeh, H., Doroudi, R., & Homami, P. (2020b). Vibration control of suspension bridge due to vertical ground motions. Advances in Structural Engineering, 23(12), 2626-2641.

28. Li, Sh., Zhang, F., Wang, J.Q., Alam, M.Sh., & Jian, Zh. (2016). Effects of Near-Fault Motions and Artificial Pulse-Type Ground Motions on Super-Span Cable-Stayed Bridge Systems. J. Bridge Eng, 22(3), 1-17.

29. Li, X., Dou, H., & Zhu, X. (2007). Engineering characteristics of near-fault vertical ground motions and their effect on the seismic response of bridges. Earthq Eng Eng Vib, 6(4), 345-350.

30. Luco, E., & Turmo, J. (2010). Linear vertical vibrations of suspension bridges: A review of continuum models and some new results. Soil Dynamics and Earthq Eng, 30, 769-781.

31. Makris, N., & Black, C.J. (2004). Dimensional analysis of rigid-plastic and elastoplastic structures under pulse-type excitations. Eng Mech, 130(9), 1006-1018.

32. Malhorta, P.K. (1999) Response of buildings to near-field pulse-like ground motions. Earthq Eng Struct Dynam, 28, 1309-1326.

33. Maniatakis, C.H.A., Taflampas, I.M., & Spyrakos, C.C. (2008). Identification of near-fault earthquake record characteristics. In: 14th World Conference on Earthquake Engineering, China.

34. McCallen, D.B., Astaneh-Asl, A., Larsen, S.C., & Hutchings, L.J. (2009). The response of long-span bridges to low frequency near-fault earthquake ground motions. TCLEE, 1-12.

35. Memarpour, M.M., Ghodrati Amiri, G., Razeghi, H., Akbarzadeh, M., & Tajik Davoudi, A. (2016). Characteristics of horizontal and vertical near-field ground motions and investigation of their effects on the dynamic response of bridges. Rehab in Civil Eng, 4(2), 1-24.

36. Murphy, T.P., & Collins, K.R. (2008). Retrofit of suspension bridges subjected to long period earthquake motion. In: 12th world conference on earthquake engineering, Auckland, New Zealand, Paper no. 2310.

37. Ohmachi, T., & Jalali, A. (1999). Fundamental study on near-fault effects on earthquake response of arch dams. Earthq Eng Eng Seismol, 1, 1–11.

38. Pacific Earthquake Engineering Research Center (PEER) http://www.peer.berkeley.edu.

39. Rodriguez, S., & Ingham, T.J. (1995). Seismic protective system for the stiffening truss of the golden gate bridge. Proceedings National Seismic Conference on highways and bridges, Federal highway administration, California.

40. Rubin, L.I., Abdel-Ghaffar, A.M., & Scanlan, R.H. (1983) Earthquake response of long span suspension bridge. 83-SM-13, Princeton university, Princeton.

41. Shrestha, B. (2015). Seismic response of long span cable-stayed bridge to near-fault vertical ground motions. KSCE Journal of Civil Engineering, 19(1), 180-187.

42. Shrestha, B., & Tuladhar, R. (2012). Response of Karnali Bridge, Nepal to near fault earthquakes. In: Proceedings of ICE- Bridge Engineering (ICE), 165(4), 223-232.

43. Somerville, P.G. (2003). Magnitude scaling of near fault rupture directivity pulse. Phys Earth Planet, 137(1), 201-212.

44. Soyluka, K., & Karaca, H. (2017). Near-fault and far-fault ground motion effects on cable-supported bridges. Procedia Eng, 199, 3077-3082.

45. Zhang, S., & Wang, G. (2013). Effects of near-fault and far-fault ground motions on nonlinear dynamic response and seismic damage of concrete gravity dams. Soil Dyn Earthq Eng, 53, 217–229.